Non-local diffusion-weighted image super-resolution using collaborative joint information

ZHIPENG YANG[1,2], PEIYU HE[1], JILIU ZHOU[3] and XI WU[3]

[1]School of Electronics and Information Engineering, Sichuan University, Chengdu, Sichuan 610065; Departments of [2]Electronic Engineering and [3]Computer Science, Chengdu University of Information Technology, Chengdu, Sichuan 610225, P.R. China

Received February 3, 2017; Accepted August 10, 2017

DOI: 10.3892/etm.2017.5430

Abstract. Due to the clinical durable scanning time and other physical constraints, the spatial resolution of diffusion-weighted magnetic resonance imaging (DWI) is highly limited. Using a post-processing method to improve the resolution of DWI holds the potential to improve the investigation of smaller white-matter structures and to reduce partial volume effects. In the present study, a novel non-local mean super-resolution method was proposed to increase the spatial resolution of DWI datasets. Based on a non-local strategy, joint information from the adjacent scanning directions was taken advantage of through the implementation of a novel weighting scheme. Besides this, an efficient rotationally invariant similarity measure was introduced for further improvement of high-resolution image reconstruction and computational efficiency. Quantitative and qualitative comparisons in synthetic and real DWI datasets demonstrated that the proposed method significantly enhanced the resolution of DWI, and is thus beneficial in improving the estimation accuracy for diffusion tensor imaging as well as high-angular resolution diffusion imaging.

Introduction

Diffusion-weighted magnetic resonance imaging (DWI) has been established as an important non-invasive technique for probing and characterizing the microstructure of living tissue *in vivo* (1). While probing the capability of water to diffuse in various directions and scales, multiple 3-dimentional (3D) DWIs have been acquired using echo-planar imaging (EPI). However, the spatial resolution and signal-to-noise ratio (SNR) is limited by several physical, clinical and economical considerations (2). Poor spatial resolution in fact poses significant limits on the scale of tissue structure that may be characterized by DWI. For instance, individual axon diameters are in the order of 1-30 μm, while the typical DWI resolution is ~2x2x2 mm^3, which only provides summative measures from millions of axons. In addition, the partial volume effect also limits the DWI to the investigation of the major fiber bundles in the brain (3). Therefore, increasing spatial resolution of DWI is beneficial for reducing partial volume effects, which allows fine details of the tissue structure to be resolved and characterized with enhanced certainty (4).

Several methods have been proposed to increase the spatial resolution of DWI, and may be broadly divided into two categories: The acquisition procedure and the post-processing procedure. Increasing spatial resolution through image acquisitions typically involves the use of high-quality diffusion gradient coils, and a longer echo time (TE) that is necessary for encoding a larger k-space in a single shot. However, increasing TE leads to increased error accumulations during spatial encoding and enhanced geometric and intensity distortion along the phase encoding direction (5). Alternatively, higher magnetic fields (7 Tesla or more) may be employed, which offers an effective solution to improving SNR while reducing image distortion caused by larger spatial encoding (6). Other methods have also been proposed for improving spatial resolution, for instance, using a specifically designed gradient coil such as Gradient Insert (7). While all these methods require a hardware upgrade in the scanner, methods that are based on changing image acquisition schemes for the purpose of improving spatial resolution are also available. A representative method of this type is anisotropic orthogonal acquisition, which employs a maximum of a posteriori estimations from multiple scans to exploit spatial homogeneity and provide regularized solutions for isotropic high-resolution (HR) (8).

Enhancing spatial resolution in the post-processing procedures shares the common concept as the well-known super-resolution (SR) technology, which was developed for the same problem in video sequences (9). A preliminary study on SR of DWI data was performed by Peled and Yeshurun (2), who resorted to a set of spatially shifted DWI for enhanced spatial resolution. Later, Arsigny *et al* (10) introduced Log-Euclidean metrics into interpolation of diffusion tensor magnetic resonance imaging (DTI) data, which naturally allows for tensor

Correspondence to: Professor Xi Wu, Department of Computer Science, Chengdu University of Information Technology, Block 1, 24 Xuefu Road, Chengdu, Sichuan 610225, P.R. China
E-mail: xi.wu@cuit.edu.cn

Key words: diffusion-weighted imaging, super-resolution, nonlocal means, joint information, rotational invariance

super-resolution. Furthermore, Calamante *et al* (11) proposed a tract density imaging-based method that weighs the interpolation with tract density, which elegantly achieves an appealing visualization effect.

Intuitively, the resolution of DWI may be enhanced by adapting state-of-the-art SR methods from simple scene images, such as the non-local method (12) and overcomplete dictionaries (13). However, as pointed out in numerous DWI applications (14-16), due to the particular nature of DWI data, only a combination of multiple channels may reveal the complex structure of white matter, since a single channel simply captures partial information regarding the underlying neuronal structure. In the present study, a novel SR method for a multiple-channel DWI dataset was proposed based on a well-known non-local mean filter. The proposed method introduced joint information, which encapsulates the intrinsic similarity redundancy of adjacent DWI channels, to improve the regularization of the SR procedure. In addition, an efficient rotational invariant similarity measure was also applied to the proposed SR method. This not only increased the redundant pattern, which is beneficial for more accurate HR image reconstruction, but also reduced the computational burden for more practical applications.

A preliminary version of the proposed method was first described in a conference paper (17). The present study consolidated this work and expanded on the results. The proposed SR method is described in detail in the method section. After quantitative and qualitative comparison of the proposed SR framework on a synthetic and a real DWI dataset, the advantages and limitations of the proposed technique were discussed.

Materials and methods

Methods. To recall the problem of SR, it may be assumed that the low-resolution (LR) image Y corresponds to the original HR image X according to the following model:

$$\mathbf{Y} = DH\mathbf{X} + \eta \quad (1)$$

where H is the degradation operator, D is the decimation operator and η is additive noise. The SR reconstruction problem is to estimate the underlying HR version $\mathbf{X}$ from $\mathbf{Y}$ as follows:

$$\hat{\mathbf{X}} = \arg\min_{\mathbf{X}} \left\| \mathbf{Y} - DH\mathbf{X} \right\|^2 + \lambda \Re(\mathbf{X}) \quad (2)$$

where $\Re(\mathbf{X})$ is a regulation term and λ is the regulation parameter that balances the fidelity term and regulation term.

A non-local strategy has been proposed primarily as an efficient denoising method (18), and was then adapted to multiply modifications (12,19-21). In addition to denoising applications, the non-local method may also be adapted for an SR reconstruction task (12,22-24). In these applications, the patch-based non-local estimator was used to define the regulation term:

$$\Re(\mathbf{X}) = \sum_{p \in \Omega} \left| \mathbf{X}_p - \hat{\mathbf{X}}_p \right| \quad (3)$$

where $\hat{\mathbf{X}}_p$ is acquired with a non-local estimator:

$$\hat{\mathbf{X}}_p = \sum_{q \in \omega} w(\mathbf{X}_p, \mathbf{X}_q)\mathbf{X}_q \quad (4)$$

in which X_p and X_q are the voxels at location p and q, respectively, ω is a searching window and w weighs the similarity betweenpatches $S(X_p)$ and $S(X_q)$ as below:

$$w(\mathbf{X}_p, \mathbf{X}_q) = \frac{1}{Z_p} e^{-\frac{\left\| S(\mathbf{X}_p) - S(\mathbf{X}_q) \right\|^2}{h^2}}$$

where h is the decay parameter and Z_p is a normalization constant that is defined as the sum of all the weights.

As previously reported (12), after computing this regularization term, the fidelity term is then applied for subsampling consistency (25):

$$\mathbf{Y}_p - \frac{1}{L}\sum_{i=1}^{L} \hat{\mathbf{X}}_p = 0, \ \forall p \in \mathbf{Y} \quad (6)$$

Finally, this non-local interpolation framework is implemented iteratively until convergence, and this two-step iteration may be defined as follows:

$$\hat{\mathbf{X}}_p^{t+1} = \frac{1}{Z_p} \sum_{q \in \omega} e^{-\frac{\left\| S(\mathbf{X}_p^t) - S(\mathbf{X}_q^t) \right\|^2}{h^2}} \mathbf{X}_q^t \quad (7)$$

$$\hat{\mathbf{X}}^{t+1} = \hat{\mathbf{X}}^{t+1} - NN(DH\hat{\mathbf{X}}^{t+1} - \mathbf{Y}) \quad (8)$$

where NN is the nearest neighbor interpolation, and t is the iteration number. Equations 7 and 8 correspond to the non-local reconstruction and mean correction, respectively.

This non-local SR method was proposed primarily for 3D MRI, and was then adapted for DWI application, which uses non-diffusion image (*b0*) information as the HR reference to guide the reconstruction (24).

Of note, joint information, as indicated previously, gathers the information from all correlated gradient images, providing extra redundancy, which is beneficial for SR reconstruction.

X^N_p and X^N_q denote the DWI patches, with N corresponding to the Nth gradient direction. Due to the fact that DWI is stored sequentially, an adjacent gradient direction is associated with a higher correlation. As previously reported (19,21), a more efficient non-local estimation may be acquired through a more accurate weighting scheme. Intuitively, it is possible for joint information from correlation gradient directions to improve weighting accuracy, which leads to better SR reconstruction:

$$(\hat{\mathbf{X}}_p^N)^{t+1} = \sum_{q \in \omega} w((\mathbf{X}_p^N)^t, (\mathbf{X}_q^N)^t)(\mathbf{X}_q^N)^t, \quad (9)$$

$$w((\mathbf{X}_p^N)^t, (\mathbf{X}_q^N)^t) = \frac{1}{Z_p} \exp\left\{ -\left(\frac{\left\| S(\mathbf{X}_p^{N-k}) - S(\mathbf{X}_q^{N-k}) \right\|^2}{h^2} + \cdots + \frac{\left\| S(\mathbf{X}_p^N) - S(\mathbf{X}_q^N) \right\|^2}{h^2} + \cdots + \frac{\left\| S(\mathbf{X}_p^{N+k}) - S(\mathbf{X}_q^{N+k}) \right\|^2}{h^2} \right) \right\} \quad (10)$$

where $k = round(\frac{n-1}{2})$, with n being a constant resembling the number of gradient directions.

It should be noted that the similarity measure in equation 10 is not rotationally invariant. As previously pointed out (19,20), the rotationally invariant measure may be applied

to the proposed SR method for further improvement of the HR image reconstruction. Manjon *et al* (19) proposed a simple but effective rotationally invariant measure, which is based on voxel intensity and the corresponding patch means. The present study we adopted this rotationally invariant measure into a non-local SR method with joint information of DWI, so that the similarity measure in equation 10 may be rewritten as follows:

$$w((\mathbf{X}_p^N)^t,(\mathbf{X}_q^N)^t)=\frac{1}{Z_p}\exp\left\{-\left(\frac{\left\|S(\mathbf{X}_p^{N-k})-S(\mathbf{X}_q^{N-k})\right\|^2}{h^2}+\cdots+\frac{\left\|S(\mathbf{X}_p^{N})-S(\mathbf{X}_q^{N})\right\|^2}{h^2}+\cdots\right.\right. \quad (11)$$
$$\left.\left.+\frac{\left\|S(\mathbf{X}_p^{N+k})-S(\mathbf{X}_q^{N+k})\right\|^2}{h^2}+\frac{3\left\|\mu((\mathbf{X}_p^N)_n)-\mu((\mathbf{X}_q^N)_n)\right\|^2}{h^2}\right)\right\}$$

where μ is the mean of the patches around voxel X_p^N (or X_q^N) and its corresponding n nearby gradient directions.

As presented in equation 8, the mean correction step in order to ensure that the reconstructed HR image is consistent with the original LR image is as follows:

$$(\hat{\mathbf{X}}^N)^{t+1}=(\hat{\mathbf{X}}^N)^{t+1}-NN(DH(\hat{\mathbf{X}}^N)^{t+1}-\mathbf{Y}) \quad (12)$$

where NN is the nearest neighbor interpolation, H is the degradation operator, D is the decimation operator and $\hat{X}^N$ is the reconstructed HR image.

Experiments. A synthetic dataset, a high-field *in vivo* DWI dataset and a physical phantom dataset were selected to evaluate the proposed method. Regarding the use of the *in vivo* dataset, the study was approved by the ethics committee of Vanderbilt University Institutional Review Board (Nashville, TN, USA). Prior to experiments, written informed consent was obtained from the participant. In addition, different interpolation methods and super-resolution methods were also involved for comparison. The first is B-spline interpolation, which was introduced for DWI resolution enhancement in the literature (26,27) and was used for comparison. A non-local approach for MRI super-resolution (12) was also involved for comparison, together with the proposed method implementing joint information (Proposed-n) and rotationally invariant similarity measure (Proposed-RI-n). For the methods used in the present study, all scenarios were tested (n=1, 3, 5), since using more gradients becomes computationally prohibitive. As presented in equation 10, if n=1, the algorithm is simplified to the classical non-local method. The searching window was set as suggested in (12), and the decremental approach alone was used in the convergence process to define the delay parameter h (24).

The simulation dataset consists of the 3D structure field presented at the 2012 high-angular resolution diffusion imaging (HARDI) Reconstruction Challenge (28) and has a 16x16x5 volume attempting to simulate a realistic 3D configuration of tracts occurring. As presented in Fig. 1A, this dataset is comprised of five different fiber bundles, which gave rise to the nonplanar configurations of bending, crossing and kissing tracts. All fiber tracts were characterized with a fractional anisotropy between 0.75 and 0.90. To better explore the proposed method, this synthetic dataset was also corrupted by Rician noise (SNR, 30) and displayed in Fig. 1F. The original dataset and the noisy one were down-sampled by a factor of 2 using the nearest neighbor interpolation along each axis. Next, the LR datasets were super-resolved using the B-spline method, the non-local method, and the proposed methods with 5 directions. In addition to the visual comparison demonstrated in Fig. 1, the angular accuracy was also involved for quantitative evaluation (28). The angular accuracy in the orientation of the estimated fiber compartments was assessed by means of the average error (in degrees) between the estimated fiber directions and the true ones present in a voxel:

$$\bar{\theta}=\frac{180}{\pi}\arccos(|\mathbf{d}_{true}\times\mathbf{d}_{estimated}|) \quad (13)$$

where the unitary vectors $\mathbf{d}_{true}$ and $\mathbf{d}_{estimated}$ are a true fiber population in the voxel and the ones closest to the estimated directions.

The *in vivo* DWI dataset was acquired by a 7T Philips Achieva whole-body scanner (Philips Healthcare, Cleveland, OH, USA) with a volume head coil for transmission and 32-channels. A DW dual spin-echo, SENSE accelerated multi-shot EPI was used to acquire the DWI data (b-value, 700 sec/mm^2; 15 diffusion directions; field of view, 210x210x30 mm^3; matrix size, 300x300 with 15 slices and a spatial resolution of 0.7x0.7x2 mm^3). A gold standard image was constructed based on this *in vivo* HR DWI dataset to quantitatively and qualitatively validate the proposed approach. For this, 10 acquisitions of HR DW images were averaged in the image space (0.7x0.7x2 mm^3). The LR images used for the experiment were then simulated by down-sampling the gold standard by a factor of 2 using the nearest neighbor interpolation along each axis, i.e., [2 2 2], which resulted in simulated LR images of 1.4x1.4x4 mm^3. The HR and LR data were filtered using the UNLM3D filter to remove random noise prior to HR reconstruction. Two objective measure matrixes, namely the Peak SNR (PSNR) and the structural similarity (SSIM) (29) were used to quantitatively evaluate the super-resolved DWI dataset. The PSNR measures the differences between each of the images and the image quality, while the SSIM measures the structure and perceptual similarities between the original and reconstructed images.

$$\mathrm{SSIM}(x,y)=\frac{(2\mu_x\mu_y)(2\sigma_{xy}+c_2)}{(\mu_x^2+\mu_y^2+c_1)(\sigma_x^2+\sigma_y^2+c_2)} \quad (14)$$

where μ_x and μ_y are the mean value of images x and y, Σ_x and Σ_y are the standard deviation of x and y, respectively, S_{xy} is the covariance between them, and constants *c1* and *c2* were set as suggested in a previous study (29).

For further investigation, a physical phantom dataset used in tracking analysis was also implemented. As proposed in previous studies (30,31), this phantom dataset was scanned in two spatial resolutions; a dataset with a resolution of 6x6x6 mm^3 was selected for interpolation and a dataset with a resolution of 3x3x3 mm^3 was used for comparison.

Finally, a diffusion tensor image (32) and a HARDI model using spherical deconvolution (33) were reconstructed using the super-resolved DWI dataset for evaluation in a quantitative as well as a qualitative manner. For a synthetic phantom, the diffusion tensor field and principal eigenvector were computed using CAMINO (34) and are displayed in Fig. 1. Table I presents the mean and standard deviation of the angular error estimated by equation 13. For the *in vivo* dataset,

the DWI reconstruction results were quantitatively and qualitatively compared in Figs. 2 and 3, respectively, followed by comparison of the effect of motion artifacts and geometric distortions in Figs. 4 and 5. Fractional anisotropy (FA), the FA-weighted color map of the principal eigenvector and the principal eigenvector of the estimated tensor and were determined and displayed in Figs. 6, 7 and 8, respectively. For the physical phantom dataset, the orientation distribution function (ODF) using spherical deconvolution (33) was estimated and displayed in Fig. 9.

All experiments were performed on a personal computer running MATLAB R2013b (Mathworks, Natick, MA, USA) in Windows 7, with an Intel(R) core i7-4600 U processor and 8 GB RAM.

Results

Simulation results. Fig. 1 demonstrates the principal eigenvector of the tensor model in the synthetic phantom and the results of the reconstruction performed using the above-mentioned methods. It was indicated that the proposed methods outperformed the interpolated method in noisy as well as no-noise situations. By carefully observing Fig. 1E and J, it may be observed that the proposed method achieved more robust reconstruction results with no irregular tensors, as indicated by arrows. This was also in accordance with the quantitative comparison of the angular error in Table I, in which the proposed method achieved the most accurate reconstruction results of tensor direction in the original and noisy datasets.

In vivo dataset results. The quality of DWI reconstruction is demonstrated in Figs. 2 and 3. Fig. 2 presents the PSNR and SSIM of the proposed method compared with B-spline interpolation and non-local upsampling (12). As indicated in the study by Manjón *et al* (12), the patch-based method was better than the classical interpolation. For the proposed method of the present study, the super-resolution using joint information enhanced the reconstructed image quantitatively for every DWI image with different directions. In addition, PSNR as well as SSIM improved with the increasing involvement of nearby DWI images. Fig. 3 presents the visual comparison of the reconstructed DWI images. The reconstructed image (Fig. 3B) had the blurriest result of all, while the proposed method using seven nearby gradient images (Fig. 3E) achieved the image most similar to the golden standard (Fig. 3A). The crack in the enlarged region demonstrates that using joint information, the proposed-RI-5 grad (Fig. 3E) reconstructed the best spatial features of the cracked area as indicated by the blue arrow, compared with the same area reconstructed by other methods, in which the edges are blurry and difficult to distinguish.

As indicated by Coupé *et al* (24), DWI datasets are vulnerable to motion artifacts and geometric distortions. Therefore, the impact of misalignments on the quality of results using the proposed method was studied. First, the displacements between b0 and DW images were obtained with an FSL eddy current correction (35) and the mean displacements estimated from the reconstruction results are displayed in Fig. 4A. Fig. 4B demonstrates the correlation between image quality in terms of PSNR and the estimated mean displacements. No significant linear correlation between the results from the proposed method and the estimated mean displacements was observed, which demonstrates the robustness of the proposed method towards the limited misalignment.

The impact of distortion corrections on the results of the proposed method was also studied in Fig. 5. The experiment in Fig. 1 was repeated using the corrected dataset, and data were then subjected to the FSL eddy current correction. Subsequently, the PSNR and SSIM of the results using B-spline, non-local upsampling and the proposed method were computed using the corrected gold standard and presented in Fig. 5.

Figs. 6 and 7 demonstrate the FA map and color map, respectively, of the estimated DTI data from the reconstructed DWI. Table II presents the PSNR and SSIM of the FA map. Consistent with Figs. 2 and 3, the FA and color map estimations using B-spline interpolation were worst among all methods. Following careful observation of the results in the boxed areas, it became apparent that the proposed method provides a better estimation for FA, application of the upsampling method resulted in coarse edges and the proposed method reconstructed the highest volume corresponding to the gold standard image. For the anterior horn of the lateral ventricle (indicated by the blue arrow) and external capsule tract (indicated by the red arrow), the artifacts introduced by upsampling methods are visible on strong edges, but these artifacts are not present when using the proposed method. Compared with the non-local upsampling method (Fig. 7C), the proposed method (Fig. 7D and E) preserved greater details along association tracts (indicated by the green arrow). The qualitative performance of proposed-5 grad (Fig. 7D) and proposed-RI-5 grad (Fig. 7E) is somewhat similar, however, this is likely due to the tolerance of the DTI reconstruction method to small quantitative differences (Fig. 2). Fig. 8 presents the principal eigenvector of the tensor around the corpus callosum for the gold standard and the compared methods. Although all five methods maintained tensor orientation of most pixels, some single fiber tensors in the corpus callosum (the region indicated by the red box) were smoothed by B-spline interpolation (Fig. 8C) and non-local upsampling (Fig. 8D), whereas this did not appear with the proposed method (Fig. 8E and F). In addition, the proposed method achieved sharper interpolation than the other methods in the fiber crossing area from the corpus callosum to the ventricle.

Physical phantom results. Fig. 9 presents the ODF obtained by spherical deconvolution for the B-spline, non-local upsampling, proposed-5 grad and proposed-RI-5 grad methods with the gold standard used as a reference. For better visualization, the regions of the sharp turn (second row) and crossing (third row) were enlarged. The B-spline interpolation was obtained over smoothed results from which a great deal of ODF information is missing. As indicated in Fig. 9J and K, the proposed method better resolves fiber sharp turn and crossing areas to facilitate fiber tracking. Circles are used to indicate the differences in performance (Fig. 9J). Close inspections reveal that the proposed-RI-5 grad better resolved the vertical component, which is represented by the green lobe of each ODF and with a stronger green lobe, better tracking of the sharp turn can be achieved.

Table I. Angular error on estimated tensors in original phantom and noisy phantom (signal-to-noise ratio, 30) using B-spline, non-local upsampling and proposed method.

Phantom	B-Spline angular error (˚)	Non-local angular error (˚)	Proposed-5 grad angular error (˚)	Proposed-RI-5 angular error (˚)
Original	8.6±24.5	7.4±20.5	7.2±20.3	7.0±20.1
Noisy	14.2±31.2	12.6±32.7	12.3±32.4	12.1±32.1

Proposed-5 grad, proposed method implementing joint information using 5 gradients; proposed-RI 5 grad, proposed method implementing rotationally invariant similarity measure using 5 gradients.

Table II. PSNR/SSIM values from the fractional anisotropy map compared between the different methods.

Parameter	B-Spline	Non-local	Proposed-5 grad	Proposed-RI-5 grad
PSNR/SSIM	22.0/0.90	22.3/0.91	23.3/0.92	24.14/0.94

PSNR, peak signal to noise ratio; SSIM, structural similarity; proposed-5 grad, proposed method implementing joint information using 5 gradients; proposed-RI 5 grad, proposed method implementing rotationally invariant similarity measure using 5 gradients.

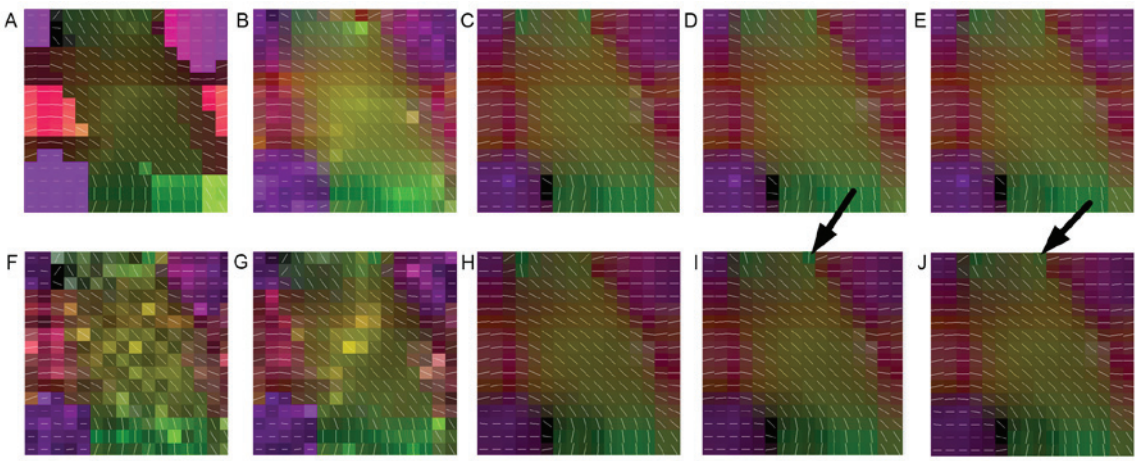

Figure 1. Principal eigenvector of tensor model in the synthetic phantom. Phantoms for (A) original dataset and datasets reconstructed using (B) B-spline, (C) non-local upsampling, (D) proposed-5 grad and (E) proposed-RI-5 grad; (F-J) noisy phantom (signal-to-noise ratio, 30); reconstructed phantom datasets for (F) the original dataset and datasets reconstructed using (G) B-spline, (H) non-local method, (I) proposed-5 grad and (J) proposed-RI-5 grad. Pixels with different results are indicated by arrows. Proposed-5 grad, proposed method implementing joint information using 5 gradients; proposed-RI 5 grad, proposed method implementing rotationally invariant similarity measure using 5 gradients.

Discussion

The present study developed a novel SR method based on a non-local mean filter to increase the spatial resolution of the DW/I dataset. The proposed method comprised an extension of the non-local SR method for more accurate HR image reconstruction using the joint information from adjacent scanning directions. Furthermore, an efficient rotationally invariant similarity measure was introduced for further improvement of the reconstruction together with reduction of computational complexity. The experimental results demonstrated that the proposed method not only improved the spatial resolution of DWI in a qualitative and quantitative manner, but also improved the estimation of diffusion parameters in DTI and HARDI.

First, the impact of the DWI direction numbers involved in the reconstruction was studied. Quantitative and qualitative experimental results demonstrated that the involvement of similarity redundancy in the nearby directions, namely joint information, allowed for a more accurate reconstruction of the DWI dataset. This is probably due to the fact that through the use of joint information, intrinsic information was retrieved from adjacent DWI channels, which is beneficial for more detailed reconstruction in the HR images. However, the increase of direction numbers is not unlimited and in the present experiment, using >5 directions did not improve the results in any notable way. This may be attributed to the fact that a similarity comparison used for the non-local super-resolution was not efficiently improved through increasing the DWI images involved, which is also in accordance with previous denoising results (16).

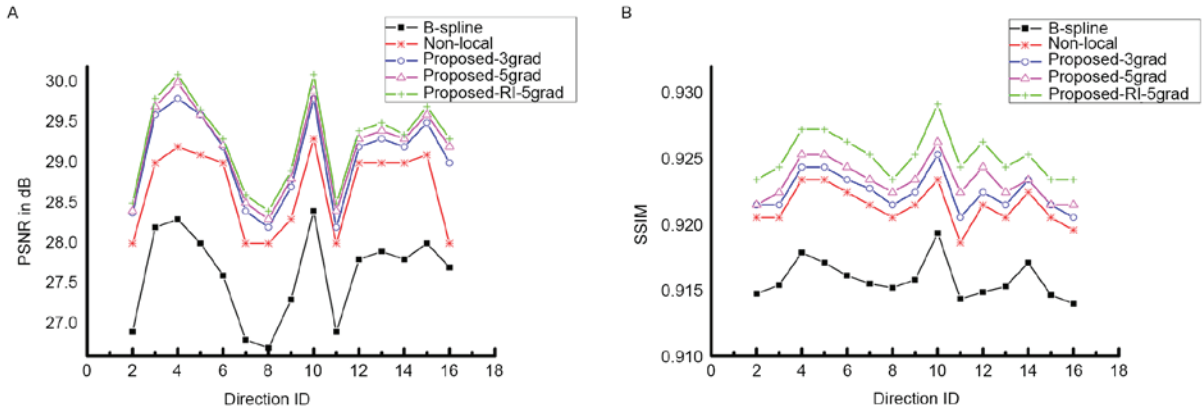

Figure 2. (A) PSNR and (B) SSIM compared between the gold standard and the images reconstructed from the simulated low-resolution image. PSNR, peak signal to noise ratio; SSIM, structural similarity. Proposed-5 grad, proposed method implementing joint information using 5 gradients; proposed-RI 5 grad, proposed method implementing rotationally invariant similarity measure using 5 gradients.

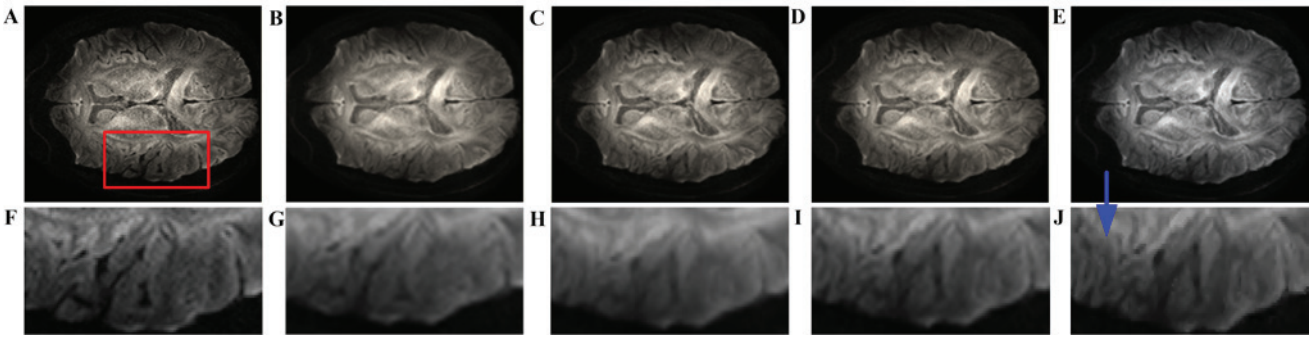

Figure 3. Comparison of diffusion-weighted image reconstruction obtained using different methods. (A) The gold standard. Results for (B) B-spline reconstruction, (C) non-local upsampling, (D) proposed-5 grad and (E) proposed-RI-5 grad. (F-J) Enlarged details for (F) the gold standard, (G) B-spline reconstruction, (H) non-local upsampling, (I) proposed-5 grad and (J) proposed-RI-5 grad. The cracked area is indicated by the blue arrow. Proposed-5 grad, proposed method implementing joint information using 5 gradients; proposed-RI 5 grad, proposed method implementing rotationally invariant similarity measure using 5 gradients.

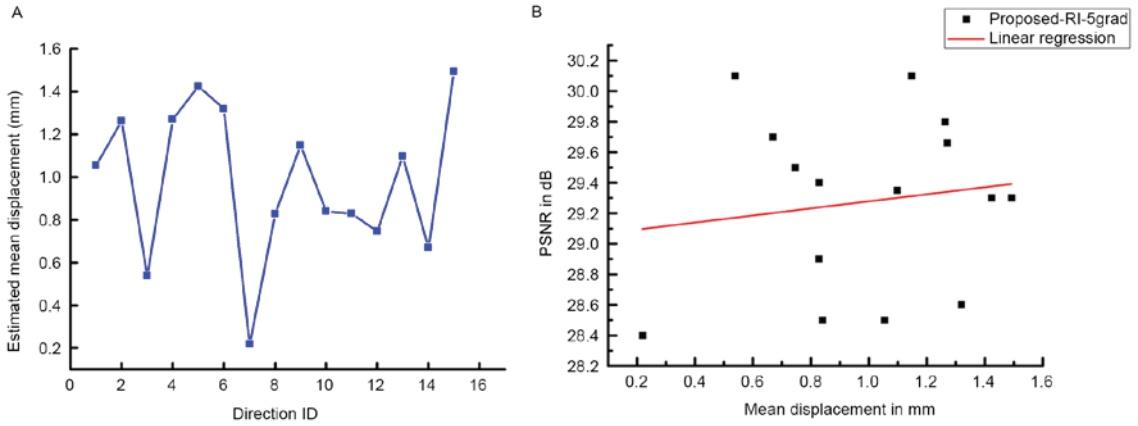

Figure 4. Effects of misalignments on the quality of results. (A) Estimated mean displacement in mm using FSL eddy current correction. (B) PSNR obtained with proposed-RI-5 grad according to estimated mean displacement. No significant linear correlation was found (P=0.51). PSNR, peak signal to noise ratio; proposed-RI 5 grad, proposed method implementing rotationally invariant similarity measure using 5 gradients.

The impact of diffusion parameter estimations was then compared. As mentioned above, the use of joint information improved the accuracy of diffusion parameter estimations using the DTI and the HARDI model, which may be beneficial for further clinical applications to image the brain in more detail. In comparison, the HARDI model is more beneficial in this framework. As indicated in Fig. 9, the estimated ODF using spherical deconvolution (33) has a more distinct geometric structure in the complex region, including crossing and sharp corners. Since the ODF estimation in a complex region remains an open problem for investigation, super-resolution using joint information may

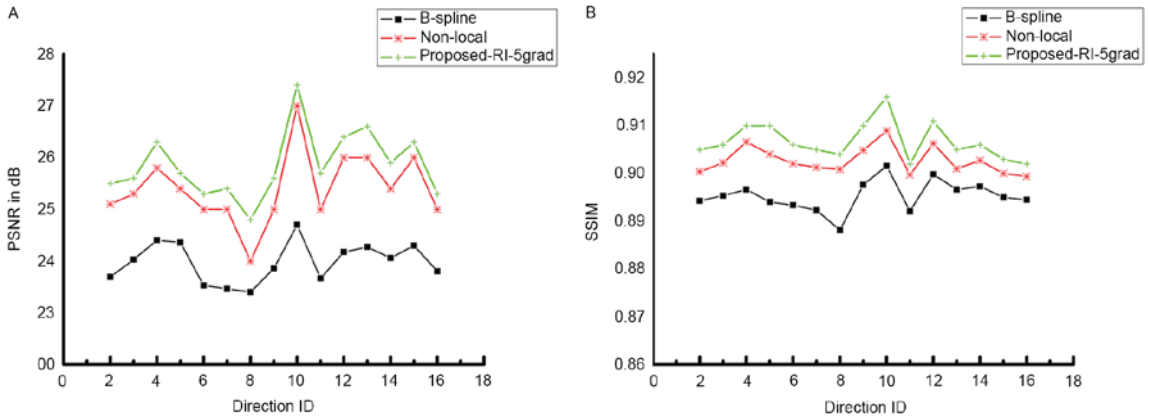

Figure 5. (A) PSNR and (B) SSIM compared between the corrected gold standard and the reconstructed images. PSNR, peak signal to noise ratio; SSIM, structural similarity. Proposed-5 grad, proposed method implementing joint information using 5 gradients; proposed-RI 5 grad, proposed method implementing rotationally invariant similarity measure using 5 gradients.

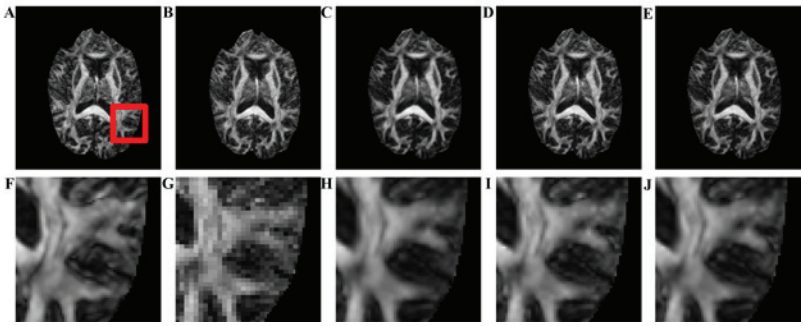

Figure 6. FA maps estimated using the gold standard and several other methods. (A) FA maps estimated for the gold standard; FA maps obtained for the reconstructed datasets of (B) B-spline reconstruction, (C) non-local upsampling, (D) proposed-5 grad and (E) proposed-RI-5 grad. (F-J) Enlarged details of (F) the gold standard, (G) B-spline reconstruction, (H) non-local upsampling, (I) proposed-5 grad and (J) proposed-RI-5 grad. Visually, the FA map obtained using the proposed method is closer to the FA of the gold standard. FA, fractional anisotropy; proposed-5 grad, proposed method implementing joint information using 5 gradients; proposed-RI 5 grad, proposed method implementing rotationally invariant similarity measure using 5 gradients.

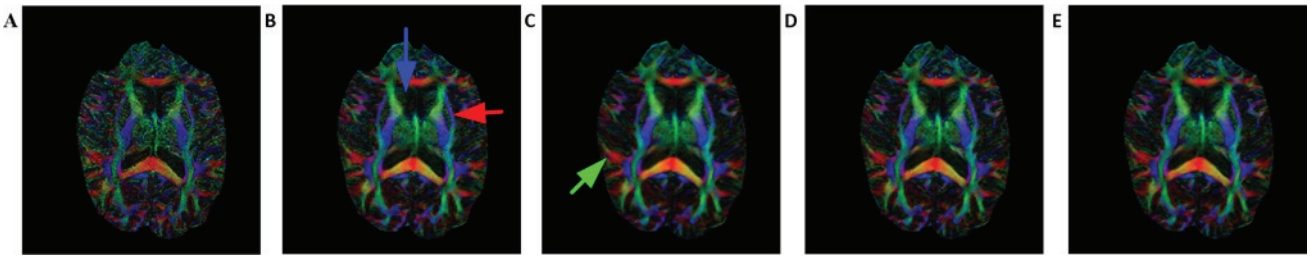

Figure 7. FA color maps estimated for the gold standard and several other methods. (A) FA color map for the gold standard; FA color map for the reconstructed dataset using (B) B-spline, (C) non-local upsampling, (D) proposed-5 grad and (E) proposed-RI-5 grad. The blue arrow indicates the anterior horn of the lateral ventricle; the red arrow indicates the external capsule and the green arrow indicates tract association tracts. FA, fractional anisotropy; proposed-5 grad, proposed method implementing joint information using 5 gradients; proposed-RI 5 grad, proposed method implementing rotationally invariant similarity measure using 5 gradients.

resemble a supplementary methodology for studies in the field.

In addition, compared with most conventional interpolation algorithms, which process each DWI component independently, the proposed method achieved notably higher-quality results, which can be contributed to two main features. Firstly, conventional interpolation techniques tend to increase the smoothness of the images, while the proposed non-local based reconstruction is highly anisotropic due to similar voxels being involved in averaging operations (12), yielding greater sharpness in the results. Secondly, a combination of all the DWI data reveals complex structures in the white matter. A significant amount of information redundancy between adjacent directions is utilized to fit the reconstruction of the white matter bundle (Figs. 6 and 7). Although the improvement is not so evident in qualitative observations from the *in vivo* experiments, the evaluation presented in Table II suggests that quantitative DTI may benefit from the joint information approaches.

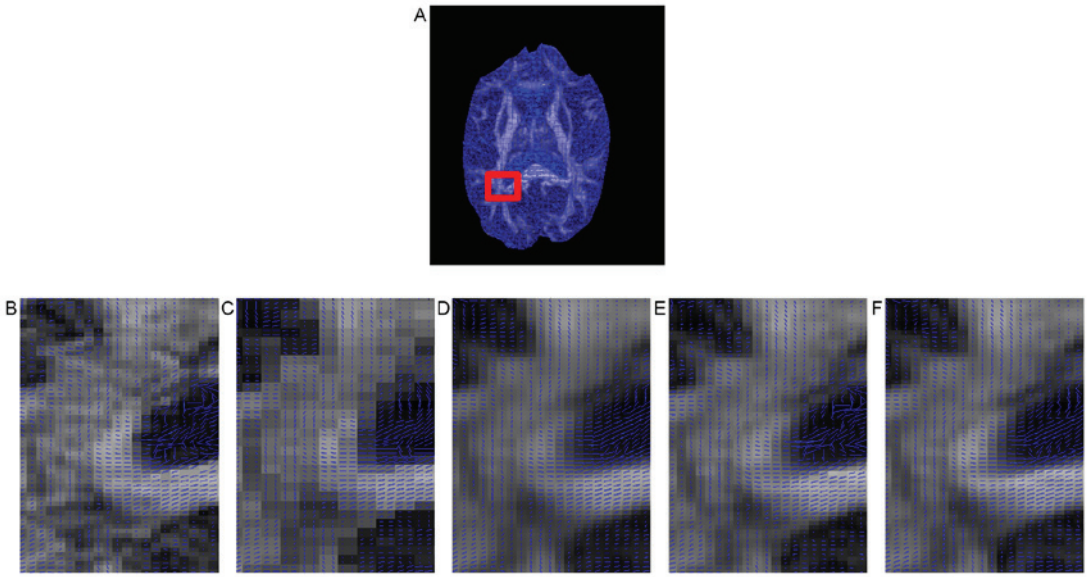

Figure 8. Diffusion tensor estimations on a central slice, centered and zoomed on the corpus callosum. (A) Tensor estimated for the gold standard. (B) Enlarged tensor estimations for the gold standard. Enlarged tensor estimations for reconstructed datasets using (C) B-spline, (D) non-local upsampling, (E) proposed-5 grad and (F) proposed-RI-5 grad. The blue lines indicate the main eigenvectors of the diffusion tensor; proposed-5 grad, proposed method implementing joint information using 5 gradients; proposed-RI 5 grad, proposed method implementing rotationally invariant similarity measure using 5 gradients.

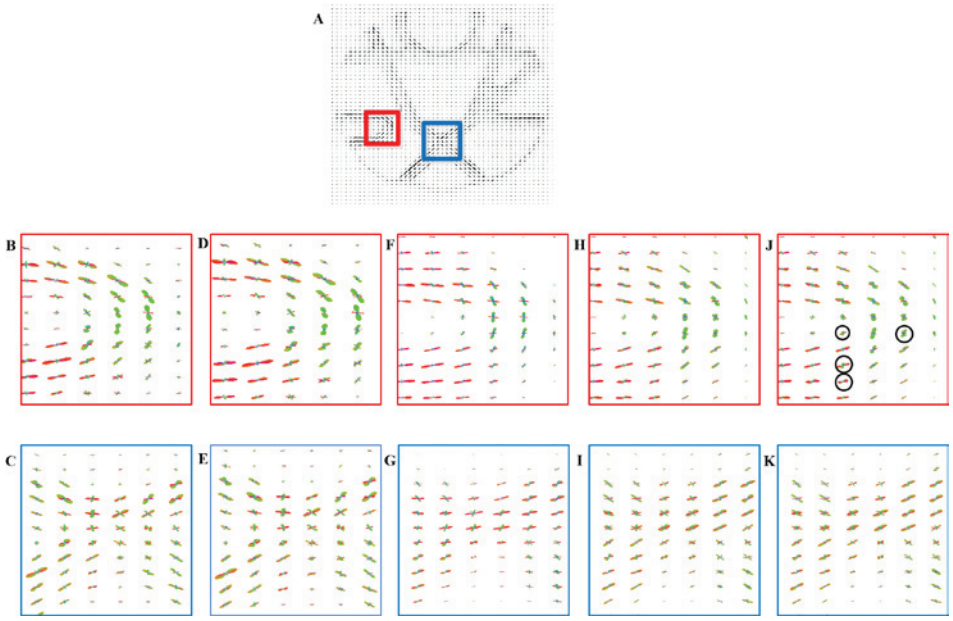

Figure 9. ODF obtained from phantom data. The images at the second row are an enlarged view of red box and third row are of blue box area. (A-C) ODF obtained with the gold standard. ODF obtained for reconstructed data set with (D and E) the B-spline, (F and G) non-local upsampling, (H and I) proposed-5 grad and (J and K) proposed-RI-5 grad. ODF, orientation distribution function; proposed-5 grad, proposed method implementing joint information using 5 gradients; proposed-RI 5 grad, proposed method implementing rotationally invariant similarity measure using 5 gradients.

Furthermore, compared with another intermodality method implemented previously (23), the method of the present study does not require any registration steps, since only the DWI dataset is required. This avoids bias introduced by registration and other modality images.

Finally, Computational complexity is another important issue for non-local based SR methods as well as DWI processing. For a typical DWI dataset with a matrix size of 128x128, 60 slices and 32 directions, the runtime for a single direction was ~8 min for non-local upsampling, 30 min for the proposed-5 grad, and 10 min for the proposed-RI-5 grad. It is expected that the implementation of parallel computing on a graphic processing unit may further speed up the reconstruction and therefore further studies focusing on this are required.

In conclusion, the present study proposed a single image non-local SR method for a DWI dataset. Compared with currently used methods, the proposed framework introduced joint information to improve the weighting scheme yet with a better image reconstruction. Furthermore, the reconstruction of the HR image was further improved by introducing

a rotationally invariant similarity measure to ensure a more accurate regularization procedure in SR and effectively reduce the computational burden. Experimentation using a synthetic as well as a real DWI dataset demonstrated that the proposed method achieved better reconstruction of detailed information in DWI and more accurate estimations of diffusion parameters from DTI and HARDI models. In addition, the present method did not require any extra data acquisition or preprocessing procedures, and may potentially improve on other super-resolution algorithms.

Acknowledgements

The present study was supported by a program of the Sichuan Science & Technology Foundation (grant no. 2017RZ0012) and a program of the National Natural Science Foundation of China (grant no. 61303126). Part of the results published in this study were previously presented at the 2015 Institute of Electrical and Electronics Engineers International Conference on Digital Signal Processing on 21-24 July 2015 in Singapore (17).

References

1. Johansen-Berg H, Behrens T and Diffusion MRI: Academic Press, New York, NY, USA, 2nd edition, 2013.
2. Peled S and Yeshurun Y: Superresolution in MRI: Application to human white matter fiber tract visualization by diffusion tensor imaging. Magn Reson Med 45: 29-35, 2001.
3. Alexander AL, Hasan KM, Lazar M, Tsuruda JS and Parker DL: Analysis of partial volume effects in diffusion-tensor MRI. Magn Reson Med 45: 770-780, 2001.
4. Mori S and van Zijl PC: Fiber tracking: Principles and strategies - a technical review. NMR Biomed 15: 468-480, 2002.
5. Miller KL, Stagg CJ, Douaud G, Jbabdi S, Smith SM, Behrens TE, Jenkinson M, Chance SA, Esiri MM, Voets NL, *et al*: Diffusion imaging of whole, post-mortem human brains on a clinical MRI scanner. Neuroimage 57: 167-181, 2011.
6. Hu X and Norris DG: Advances in high-field magnetic resonance imaging. Annu Rev Biomed Eng 6: 157, 2004.
7. Kimmlingen R, Eberlein E, Gebhardt M, Hartinger B, Ladebeck R, Lazar R, Reese T, Riegler J, Schmitt F, Sorensen GA, *et al*: An easy to exchange high performance head gradient insert for a 3T whole body MRI system: First results. Proc Intl Soc Mag Reson Med 11: 1630, 2004.
8. Scherrer B, Gholipour A and Warfield SK: Super-resolution reconstruction to increase the spatial resolution of diffusion weighted images from orthogonal anisotropic acquisitions. Med Image Anal 16: 1465-1476, 2012.
9. Irani M and Peleg S: Motion analysis for image enhancement: Resolution, occlusion and transparency. J Vis Commun Image R 4: 324-335, 1993.
10. Arsigny V, Fillard P, Pennec X and Ayache N: Log-Euclidean metrics for fast and simple calculus on diffusion tensors. Magn Reson Med 56: 411-421, 2006.
11. Calamante F, Tournier JD, Jackson GD and Connelly A: Track-density imaging (TDI): Super-resolution white matter imaging using whole-brain track-density mapping. Neuroimage 53: 1233-1243, 2010.
12. Manjón JV, Coupé P, Buades A, Fonov V, Louis Collins D and Robles M: Non-local MRI upsampling. Med Image Anal 14: 784-792, 2010.
13. Rueda A, Malpica N and Romero E: Single-image super-resolution of brain MR images using overcomplete dictionaries. Med Image Anal 17: 113-132, 2013.
14. Fillard P, Pennec X, Arsigny V and Ayache N: Clinical DT-MRI estimation, smoothing and fiber tracking with log-euclidean metrics. IEEE Trans Med Imaging 26: 1472-1482, 2007.
15. Tristán-Vega A, Westin CF and Aja-Fernández S: A new methodology for the estimation of fiber populations in the white matter of the brain with the Funk-Radon transform. Neuroimage 49: 1301-1315, 2010.
16. Tristán-Vega A and Aja-Fernández S: DWI filtering using joint information for DTI and HARDI. Med Image Anal 14: 205-218, 2010.
17. Yang Z and He P: Non-local diffusion weighted image super-resolution using collaborative joint information. Digital Signal Processing (DSP) IEEE: 268-273, 2015.
18. Buades A, Coll B and Morel JM: A non-local algorithm for image denoising. Computer Vision and Pattern Recognition, 2005. CVPR 2005. IEEE Computer Society Conference on, 2005. Doi: 10.1109/CVPR.2005.38.
19. Manjón JV, Coupé P, Buades A, Louis Collins D and Robles M: New methods for MRI denoising based on sparseness and self-similarity. Med Image Anal 16: 18-27, 2012.
20. Lou Y, Favaro P, Soatto S and Bertozzi A: Nonlocal similarity image filtering. In Image Analysis and Processing - ICIAP 2009-15th International Conference, Proceedings 5716: 62-71, 2009.
21. Wu X, Liu S, Wu M, Sun H, Zhou J, Gong Q and Ding Z: Nonlocal denoising using anisotropic structure tensor for 3D MRI. Med Phys 40: 101904, 2013.
22. Rousseau F: Brain hallucination. Computer Vision-ECCV 5302: 497-508, 2008.
23. Rousseau F; Alzheimer's Disease Neuroimaging Initiative: A non-local approach for image super-resolution using intermodality priors. Med Image Anal 14: 594-605, 2010.
24. Coupé P, Manjón JV, Chamberland M, Descoteaux M and Hiba B: Collaborative patch-based super-resolution for diffusion-weighted images. Neuroimage 83: 245-261, 2013.
25. Banerjee J and Jawahar CV: Super-resolution of text images using edge-directed tangent field. In DAS: 76-83, 2008.
26. Tournier JD, Calamante F and Connelly A: MRtrix: Diffusion tractography in crossing fiber regions. Int J Imaging Syst Technol 22: 53-66, 2012.
27. Raffelt D, Tournier JD, Rose S, Ridgway GR, Henderson R, Crozier S, Salvado O and Connelly A: Apparent fibre density: A novel measure for the analysis of diffusion-weighted magnetic resonance images. Neuroimage 59: 3976-3994, 2012.
28. Daducci A, Canales-Rodríguez EJ, Descoteaux M, Garyfallidis E, Gur Y, Lin YC, Mani M, Merlet S, Paquette M, Ramirez-Manzanares A, *et al*: Quantitative comparison of reconstruction methods for intra-voxel fiber recovery from diffusion MRI. IEEE Trans Med Imaging 33: 384-399, 2014.
29. Wang Z, Bovik AC, Sheikh HR and Simoncelli EP: Image quality assessment: From error visibility to structural similarity. IEEE Trans on Image Process 13: 600-612, 2004.
30. Fillard P, Descoteaux M, Goh A, Gouttard S, Jeurissen B, Malcolm J, Ramirez-Manzanares A, Reisert M, Sakaie K, Tensaouti F, *et al*: Quantitative evaluation of 10 tractography algorithms on a realistic diffusion MR phantom. Neuroimage 56: 220-234, 2011.
31. Poupon C, Rieul B, Kezele I, Perrin M, Poupon F and Mangin JF: New diffusion phantoms dedicated to the study and validation of high-angular resolution diffusion imaging (HARDI) models. Magn Reson Med 60: 1276-1283, 2008.
32. Basser PJ, Matiello J and Bihan DL: Estimation of the effective self-diffusion tensor from the NMR spin echo. J Magn Reson B 103: 247-254, 1994.
33. Tournier JD, Calamante F and Connelly A: Robust determination of the fibre orientation distribution in diffusion MRI: Non-negativity constrained super-resolved spherical deconvolution. Neuroimage 35: 1459-1472, 2007;.
34. Basser PJ, Mattielo J and LeBihan D: Estimation of the effective self-diffusion tensor from the NMR spin echo. J Magn Reson B 103: 247-254, 1994.
35. Smith SM, Jenkinson M, Woolrich MW, Beckmann CF, Behrens TE, Johansen-Berg H, Bannister PR, De Luca M, Drobnjak I, Flitney DE, *et al*: Advances in functional and structural MR image analysis and implementation as FSL. Neuroimage 23 (Suppl 1): S208-S219, 1994.